

## ARTICLE

# Bio-inspired iron/sulfur/graphene nanocomposite and its use in the catalysis of the oxygen reduction reaction at room temperature in alkaline media on a glassy carbon electrode

Behnam Seyyedi | Bahar Ahmadi Variani | Esmail Habibi

Nanotechnology Research Centre, Urmia University, Urmia, Iran

**Correspondence**Behnam Seyyedi, Nanotechnology Research Centre, Urmia University, Shahid Beheshti Avenue, Urmia 5715944931-165, Iran.  
Email: b.seyyedi@urmia.ac.ir

This work demonstrates the performance of a bio-inspired iron/sulfur/graphene nanocomposite as a non-platinum electrocatalyst for the oxygen reduction reaction (ORR) in an alkaline medium. The catalyst shows the most positive ORR onset potential (1.1 V vs. RHE) according to its unique structure in the alkaline medium (KOH solution, pH = 13) at low temperature ( $T = 298$  K). The catalyst is evaluated by the rotating-disk electrode (RDE) method under various rotating speeds (0–2,000 rpm) in the potential range  $-0.02$ – $1.18$  V vs. a rechargeable hydrogen electrode (RHE). The number of transferred electrons, as one of the most important parameters, is almost constant over a wide range of potentials (0.1–0.8 V), which indicates a more efficient four-electron pathway from  $O_2$  to  $H_2O$  on the FePc-S-Gr surface. The mean size of catalyst centers are in the nanoscale ( $<10$  nm). The estimated Tafel slope in the appropriate range is about  $-110$  mV per decade at low current density, and  $E_{1/2}$  of FePc-S-Gr displays a negative shift of only 7.1 mV after 10,000 cycles.

**KEYWORDS**

electrocatalyst, fuel cell, graphene, iron phthalocyanine, nanomaterial, non-noble metal, oxygen reduction reaction

## 1 | INTRODUCTION

Graphene is defined as an ordinary and regular two-dimensional (2D) structure consisting of an isolated, single layer of carbon in a honeycomb structure, which has unique and significant features. Graphene's noteworthy attributes include long-term operational stability, high strength, economy, and good conductivity for electricity and heat.<sup>[1–5]</sup> Because of its good electrical conductivity, graphene is a suitable candidate as a substrate for non-precious-metal catalysts (NPMCs). NPMCs supported by carbon, including graphene, are a serious possible alternative for platinum catalysts. Because of the slow kinetics of the oxygen reduction reaction (ORR), platinum and its derivative are widely used as catalysts for ORR; however, these have considerable

limitations. ORR plays an important role in electrochemical energy generation and storage systems (such as fuel cells and Li-ion batteries), which are rapidly developing. The fuel cell, as a next-generation energy system, supplies electricity by the conversion of chemical energy, and its performance is strongly dependent on the ORR kinetics.<sup>[6–11]</sup> Extensive research has been carried out to develop various NPMCs for ORR.<sup>[12–16]</sup> Since different electrocatalysts lead the ORR in aqueous solutions through two pathways, many precursors have been introduced with different performances – either through an efficient two-step, two-electron pathway from  $O_2$  to hydrogen peroxide, or a more efficient four-electron way from  $O_2$  to  $H_2O$ .<sup>[17–19]</sup> Recently, many studies have shown that the M-N<sub>4</sub>-C structure is the most efficient catalyst for ORR, where M is a transition metal such as iron, copper,

cobalt, or zinc.<sup>[20–24]</sup> In this context, the cytochrome enzyme is a promising material for electrocatalysis of ORR in nature. Cytochrome uses iron atoms in the form of Fe (N<sub>4</sub>) as catalyst for oxygen reduction.<sup>[25]</sup> In this work, the Fe (N<sub>4</sub>) centers are stabilized by the iron phthalocyanine structure. Phthalocyanines and their derivatives are a widely investigated as important functional materials. Metal phthalocyanines, as 2D metal-organic materials, form M (N<sub>4</sub>) centers with most transition metals; moreover, they have been investigated as catalysts for various reactions including ORR and redox systems. Although metal phthalocyanines and their derivatives have not been commercialized as catalysts, they have often been investigated in the several applications because of their chemical and thermal stability and specific properties.<sup>[26–32]</sup>

This study demonstrates a bio-inspired, high-performance, iron-based catalyst for ORR in alkaline media (KOH, 0.1 mol/L) at low temperature. The performance of the new bio-inspired catalyst (FePc-S-Gr) is compared with those of iron phthalocyanine (FePc) and platinum (Pt<sub>0.2</sub>/C<sub>0.8</sub>) electrocatalysts. The new catalyst is found to give a much higher ORR activity than metal-free organic N-C and Pt-based catalysts in alkaline electrolytes: especially, it is considerable in terms of  $E_{\text{Onset}}$ ,  $E_{1/2}$ ,  $n$  (the number of transferred electrons), Tafel slope, and catalyst durability. Elemental microanalysis, thermogravimetric analysis (TGA), inductively coupled plasma (ICP) analysis, Fourier transform infrared (FT-IR) spectroscopy, powder X-ray diffraction (PXRD), transmission electron microscopy (TEM), and scanning electron microscopy (SEM) were employed to evaluate the catalyst's structure.

## 2 | EXPERIMENTAL

### 2.1 | Reagents and materials

All chemicals were of analytical grade purchased from Sigma-Aldrich and used without further purification. All electrodes used were bought from Tianjin Aida Co., Ltd (China). Deionized water was used to prepare the aqueous solutions.

### 2.2 | Preparation of FePc and FePc-S-Gr

FePc was synthesized using a simple microwave oven under atmospheric pressure. Water used in the synthesis was distilled before use. A mixture of iron(II) chloride, high-purity urea, and phthalic anhydride in the weight ratio 1:4:4 was dissolved in a saturated solution of NaCl (25 mL). Next, 100 mg ammonium molybdate as catalyst and 0.5 mmol lauric acid as capping agent to suppress the flocculation of nanoparticles were added to the solution. The chemicals were dissolved in a beaker and reacted using a microwave oven (Samsung-900 W) at a low temperature (100–125°C)

for 10 min. The FePc powder was filtered, washed, and dried in an air oven at 80°C overnight. Elemental microanalysis (using a Flash EA112 automatic elemental analyzer) was used for analyzing the synthesized FePc (%), and the results are as follows: Fe 5.38; C 36.55; N 10.62; Cl 47.31; and H 0.14. The elemental mass percentages for iron (Fe%), carbon (C%), nitrogen (N%), chlorine (Cl%), and hydrogen (H%) were calculated by the following equations:

$$\text{Fe}\% = \left[ \frac{M_{\text{Fe}} \times 1}{M_{\text{FePc}}} \right] \times 100, \quad (1)$$

$$\text{C}\% = \left[ \frac{M_{\text{C}} \times 32}{M_{\text{FePc}}} \right] \times 100, \quad (2)$$

$$\text{N}\% = \left[ \frac{M_{\text{N}} \times 8}{M_{\text{FePc}}} \right] \times 100, \quad (3)$$

$$\text{Cl}\% = \left[ \frac{M_{\text{Cl}} \times (16-x)}{M_{\text{FePc}}} \right] \times 100, \quad (4)$$

$$\text{H}\% = \left[ \frac{M_{\text{H}} \times x}{M_{\text{FePc}}} \right] \times 100, \quad (5)$$

where  $M_{\text{Fe}}$ ,  $M_{\text{C}}$ ,  $M_{\text{N}}$ ,  $M_{\text{Cl}}$ ,  $M_{\text{H}}$ , and  $M_{\text{FePc}}$  are the molar mass of iron, carbon, nitrogen, chlorine, hydrogen, and FePc ( $\text{FeC}_{32}\text{N}_8\text{H}_x\text{Cl}_{16-x}$ ), respectively, and  $n$  is the number of chlorine atoms in the FePc structure. Results of the comparison of experimental and theoretical data for the elemental microanalysis of the prepared FePc shows the value of  $x$  as  $\sim 2$ .

The synthesis of the catalyst (FePc-S-Gr) included the following steps. First, about 75 mmol of Na<sub>2</sub>S was added to 75 mL of dimethylformamide (DMF) to obtain a solution; after that, the temperature was decreased to  $-5^\circ\text{C}$  in an ice bath. Then, about 75 mmol of dried graphene was broadcast into the solution, and the mixture was reacted at  $-5^\circ\text{C}$  for 12 hr. The obtained samples were filtered, washed, and dried in an air oven at 80°C overnight. To prepare FePc-S-Gr, 500 mg of the dried powder and 500 mg of the obtained FePc were dispersed in DMF (75 mL) and then cooled to  $-5^\circ\text{C}$ . The mixture was allowed to react for 24 hr. The FePc-S-Gr powder was filtered, washed, and dried in an air oven at 80°C overnight.

### 2.3 | Characterization

The FT-IR spectra for graphene, FePc-S-Gr, and FePc were recorded using a ThermoNicolet (model NEXUS FT-IR 670) spectrometer between 4,000 and 400  $\text{cm}^{-1}$  with the standard KBr pellet method. XRD patterns of FePc, graphene, and FePc-S-Gr were obtained using an X'Pert Pro-Panalytical diffractometer with Cu K $\alpha$  radiation (wavelength = 1.54 Å) at room temperature. The  $2\theta$  angular data were collected between  $2^\circ$  and  $80^\circ$  at the scan rate of  $1^\circ$  per step. To determine the Fe loading weight to the final ORR iron-based catalyst, the amounts of iron and sulfur in the

obtained FePc-S-Gr sample were analyzed by an ICP optical emission spectrometer (ICP-OES) using an ICP-MS 7900 (Agilent) (Fe: 14,071 ppm and S: 8,046 ppm) instrument. The catalyst particles size and morphology were studied by SEM and TEM using an FESEM-MIRA III (TESCAN) and EM10C-100 kV (Zeiss), microscopes, respectively.

The catalytic performance of the obtained samples for ORR was evaluated by liner sweep voltammetry (LSV) and cyclic voltammetry (CV) using an Autolab PGSTAT302N potentiostat/galvanostat. The measurements were done by employing a conventional three-electrode cell. Next, a glassy carbon rod (2 mm diameter) was used as the counter electrode<sup>[33]</sup> and a Ag/AgCl electrode was employed as the reference electrode. Afterward, a catalyst-film-coated glassy carbon rotating-disk electrode (RDE) with a surface area of 0.19625 cm<sup>2</sup> was used as a beneficial electrode. The catalyst ink was produced by adding 2 mg of the obtained powder to a solution containing 50  $\mu$ L Nafion (5 wt%) and 450  $\mu$ L deionized water. Moreover, the suspension was sonicated for 30 min. In the next step, 20  $\mu$ L of the catalyst ink was placed on the RDE surface and dried slowly to form the dry catalyst film (catalyst loading  $\approx$ 0.4 mg/cm<sup>2</sup>). Additionally, CVs and LSVs were performed in an O<sub>2</sub>-saturated KOH (0.1 mol/L) solution by varying the potential from -0.02 to 1.18 V vs. a reversible hydrogen electrode (RHE) at the scan rate of 50 and 10 mV/s, respectively. Also, the electrolyte temperature was maintained at 25  $\pm$  1°C and the background CV and LSV measurements were performed in the N<sub>2</sub>-saturated KOH (0.1 mol/L) solution.

### 3 | RESULTS AND DISCUSSION

#### 3.1 | Powder X-ray diffraction

PXRD was used to study the crystal phase structures of FePc, graphene, and FePc-S-Gr, which are shown in Figure 1.

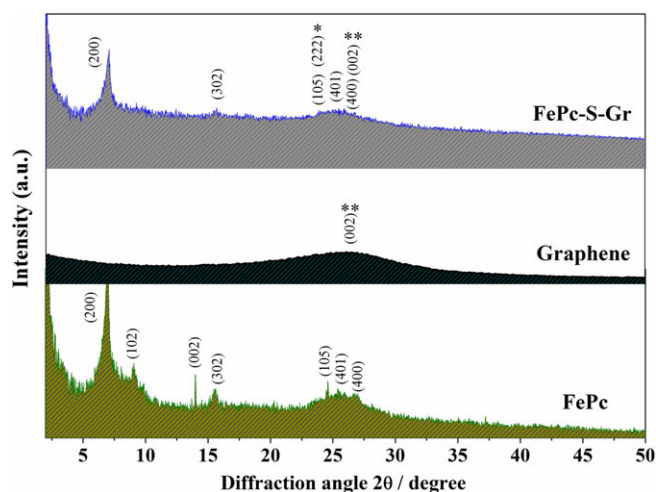


FIGURE 1 XRD pattern of graphene, FePc-S-Gr, and FePc

In general, FePc has different crystal phases, and the two peaks at  $2\theta = 6.9^\circ$  and  $9.1^\circ$  at room temperature correspond to the  $\alpha$ -FePc phase and monoclinic crystal system in the (200) and (102) planes, respectively.<sup>[34,35]</sup> The FePc and FePc-S-Gr diffraction patterns represent the peaks at  $6.9^\circ$ ,  $15.6^\circ$ ,  $24.6^\circ$ , and  $25.4^\circ$  with different intensities identical to those of  $\alpha$ -phase and monoclinic FePc (JCPDS Card No 14-0926).<sup>[36,37]</sup> The average size of the FePc and FePc-S-Gr grids,  $D$ , along the (200) direction was estimated from the Debye–Scherer equation:

$$D = \frac{0.9\lambda}{\beta \cdot \cos\theta}, \quad (6)$$

where  $\theta$ ,  $\lambda$ ,  $\beta$ , and  $D$  are the angle of incidence, the wavelength of the radiation, full width at half-maximum (FWHM in radians), and the crystalline grid size, respectively. The mean size of crystalline domains was calculated for  $\alpha$ -FePc as  $\sim$ 0.19 nm and for FePc-S-Gr  $\sim$ 0.21 nm; the difference in the crystalline grid size could be due to the sulfur bridge between  $\alpha$ -FePc and graphene. The FePc-S-Gr XRD pattern shows a diffraction peak at  $2\theta = 22.69^\circ$ , coinciding with the sulfur-carbon value.<sup>[38]</sup>

#### 3.2 | FT-IR spectrum

To locate the functional groups of FePc, Figure 2 displays the FT-IR spectra of FePc, graphene, and FePc-S-Gr with a resolution of 2 cm<sup>-1</sup> in the region of fundamental frequencies from 400 to 4,000 cm<sup>-1</sup>.

It is quite clear that IR spectral matching cannot be achieved because of the strong couplings. The band appearing at  $\sim$ 3,444 cm<sup>-1</sup> in the infrared spectra of graphene and FePc-S-Gr was assigned to an OH vibration of adsorbed water.<sup>[39]</sup> The NH stretching and bending vibrations were not observed at  $\sim$ 3,289 and 1,006 cm<sup>-1</sup>, respectively, in FePc and FePc-S-Gr. The absence of these bands is due to the replacement of hydrogen by the iron cation. The C–H stretching vibrations of the benzene rings are observed at  $\sim$ 3,028 cm<sup>-1</sup> (FePc and FePc-S-Gr). The C–C stretching

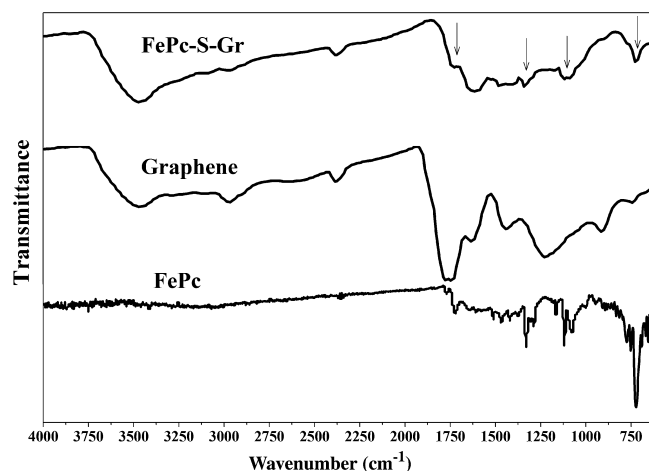


FIGURE 2 FTIR spectra of FePc, graphene, and FePc-S-Gr

vibrations of pyrrole and isoindole structures in the phthalocyanine skeleton are observing at  $\sim 1,643$ ,  $1,458$ ,  $1,376$ ,  $1,183$ ,  $1,131$ ,  $1,079$ ,  $885$ , and  $655\text{ cm}^{-1}$ . The C–H in-plane bending vibrations of the aryl structure appear at  $1,470$  and  $1,536\text{ cm}^{-1}$ . The peaks at  $1,440$  and  $1,291\text{ cm}^{-1}$  determine the =N–C bond and the stretching vibration of aromatic phenyl ring. The complex bands appearing at  $700\text{--}1,400\text{ cm}^{-1}$  were assigned to C–N in isoindole, C–Cl, and C–S stretching vibration, the C–H in-plane bending vibrations, and the C–H out-of-plane bending vibrations.<sup>[38,40,41]</sup>

### 3.3 | SEM and TEM characterization

Figure 3e–g shows the microstructure images of the FePc-S-Gr catalyst, which was obtained by a field-emission SEM. A network structure of FePc-S-Gr consisting of randomly crumpled sheets was observed in the form of a multi-layer solid, which might be attributed to the presence of foreign sulfur atoms. The TEM images indicate the homogeneously amorphous texture of graphene in which the Fe ( $N_4$ ) centers with diameter less than  $20\text{ nm}$  are deposited on the surface of the carbon particles (Figure 3a–c)

### 3.4 | Thermogravimetric analysis

TGA results obtained in air atmosphere shows the oxidation behavior of FePc, FePc-S-Gr, and graphene. The samples

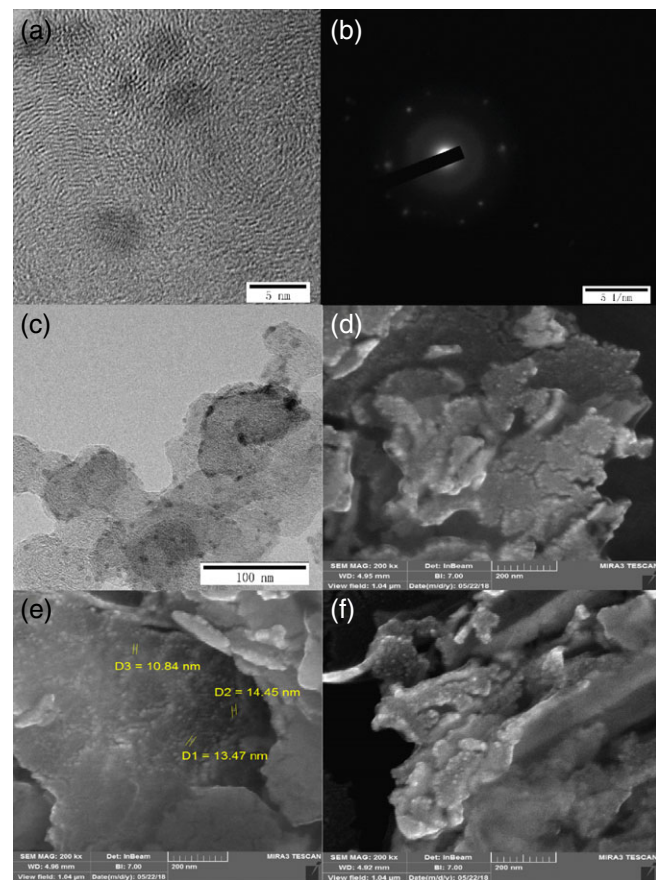


**FIGURE 3** SEM (d–f) and TEM (a–c) images of the synthesized FePc-S-Gr

were used in the temperature range  $25\text{--}800^\circ\text{C}$ . The heating rate and fluid flow were  $10^\circ\text{C}/\text{min}$  and  $50\text{ mL}/\text{min}$ , respectively (Figure 4).

Steps of weight change, loss of moisture, and thermal decomposition indicate the thermal behavior of the samples. The first step of weight change for FePc, due to the loss of moisture, occurs at  $100\text{--}150^\circ\text{C}$  (Figure 4b). Figure 4b–d shows the oxidation steps of FePc, FePc-S-Gr, and graphene, respectively. At different steps of oxidation reactions, nitrogen, carbon, chlorine, and iron atoms are oxidized. The second step of changes in Figure 4c shows the decomposition of connected FePc on graphene sheets, which does not appear in Figure 4d for graphene.

### 3.5 | Electrochemical evaluation for ORR

CVs of FePc and FePc-S-Gr in  $\text{O}_2$ -saturated KOH solution were measured at the scan rate of  $50\text{ mV}/\text{s}$  (Figure 5).

FePc shows a weak peak in the  $\text{O}_2$ -saturated solution, due to ORR activity, at about  $0.8\text{ V}$ , while for FePc-S-Gr, a well-defined cathodic peak appears, which indicates the excellent catalytic performance for ORR. To further investigate the ORR performance, RDE curves were obtained for FePc-S-Gr at various rotation rates ( $200\text{--}2,000\text{ rpm}$ ). Figure 6 shows the onset potential of the catalyst for the ORR of  $\sim 1.1\text{ V}$  (vs. RHE) after correcting for the background current at  $i_{\text{ORR}} = -0.02\text{ mA}/\text{cm}^2$ . The number of transferred electrons ( $n$ ) of the Fe-S-Gr catalyst was calculated by using the Koutecky–Levich (K–L) equation<sup>[42]</sup>

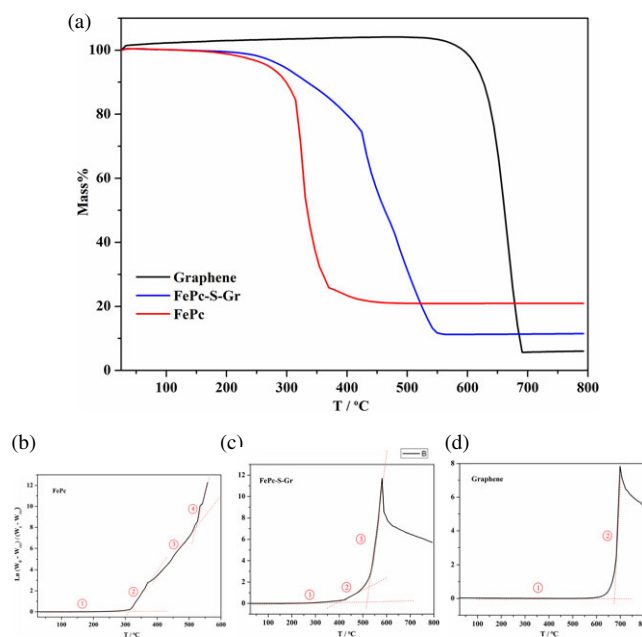


**FIGURE 4** (a) Thermogravimetric analysis of the samples in air. (b–d) Relation of  $\ln[(W_0/W_\infty)/(W/W_\infty)]$  vs temperature of chlorinated FePc, FePc-S-Gr, and graphene in air atmosphere

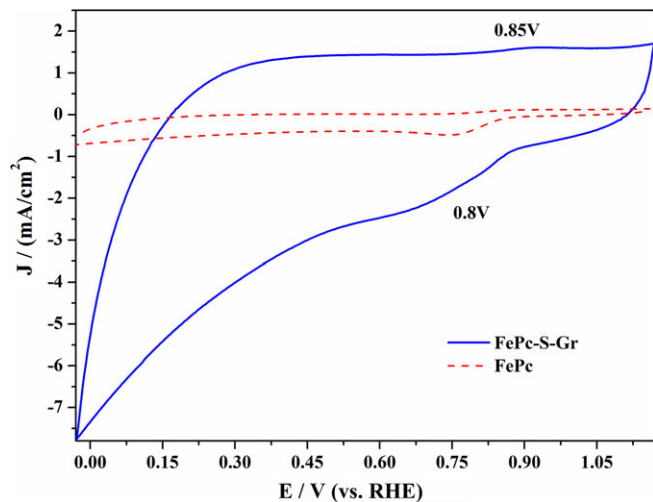


FIGURE 5 Cyclic voltammograms of the synthesized samples

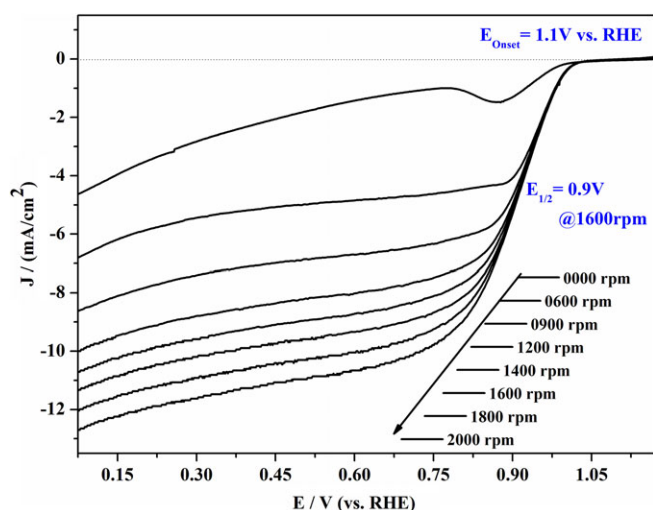


FIGURE 6 Polarization curves for catalyst performance at various rotating rates

$$J^{-1} = J_L^{-1} + J_K^{-1} = \frac{1}{B\omega^{0.5}} + \frac{1}{J_K}, B$$

$$= (0.201) \cdot n \cdot F \cdot C_{O_2} \cdot \sqrt[3]{D_{O_2}^2 \cdot 1} \cdot \sqrt[6]{\nu}, \quad (7)$$

where  $J$  is the measured current density,  $J_k$  is the kinetic current density, and  $\omega$  is the rotation rate of the electrode ( $F = 96,485 \text{ C/mol}$ ,  $C_{O_2} = 1.2 \times 10^{-6} \text{ mol/L}$ ,  $D_{O_2} = 1.9 \times 10^{-5} \text{ cm}^2/\text{s}$ ,  $\nu = 0.01 \text{ cm}^2/\text{s}$ ).

The K–L plots were obtained for the ORR on a synthesized sample (Figure 7). Using Equation (6), the slopes remain approximately constant over the potential range 0.1–0.6 V. The number of transferred electrons ( $n$ ) for FePc-S-Gr is close to 4 (Table 1).

Figure 8 shows the calculated Tafel slopes for FePc-S-Gr. The electrocatalytic activity of the sample for ORR is reflected by its Tafel slope of the diffusion-corrected kinetic current density.

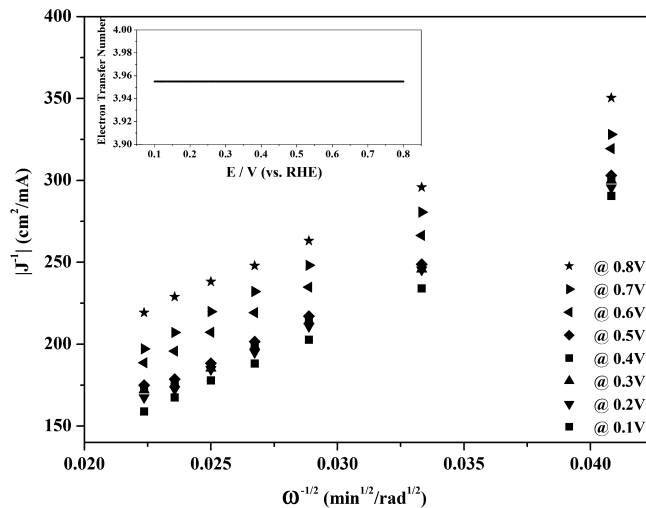


FIGURE 7 K–L plots for FePc-S-Gr

TABLE 1 Number of electrons transferred of FePc-S-Gr

$E$ (V)	$n$
0.1 V ( $J^{-1} = 7,084.7x - 0.307, R^2 = 0.9991$ )	3.96
0.2 V ( $J^{-1} = 7,080.8x + 7.2175, R^2 = 0.9988$ )	3.96
0.3 V ( $J^{-1} = 7,088.1x + 9.8428, R^2 = 0.9984$ )	3.95
0.4 V ( $J^{-1} = 7,088.1x + 10.843, R^2 = 0.9984$ )	3.95
0.5 V ( $J^{-1} = 7,088.1x + 12.843, R^2 = 0.9984$ )	3.95
0.6 V ( $J^{-1} = 7,115.3x + 29.09, R^2 = 0.9999$ )	3.94
0.7 V ( $J^{-1} = 7,080.7x + 41.766, R^2 = 0.9974$ )	3.96
0.8 V ( $J^{-1} = 7,072.1x + 60.63, R^2 = 0.9991$ )	3.96

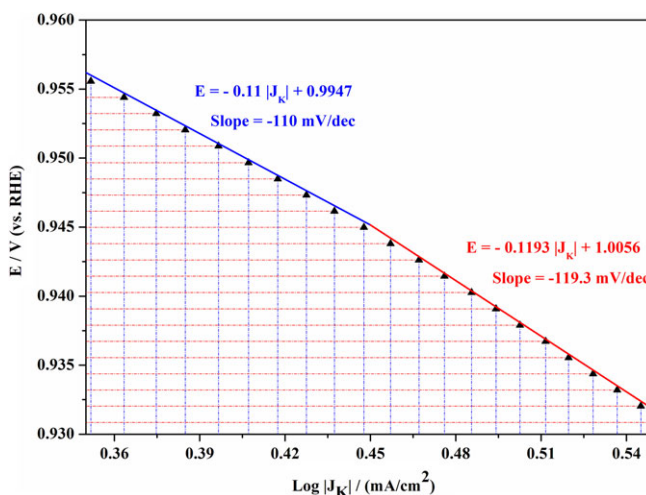


FIGURE 8 Calculated Tafel slope for FePc-S-Gr

A Tafel slope of  $-110 \text{ mV/dec}$  was observed at low current density (high potential) and of  $-119.3 \text{ mV/dec}$  was obtained in the high current density range (low potential). To be clear, the Tafel slope of commercial Pt/C is  $\sim 60 \text{ mV}$  and  $120 \text{ dec}^{-1}$ ,<sup>[42]</sup> which would be used as a reference. Principally, the range of Tafel slope for ORR is between 30 and

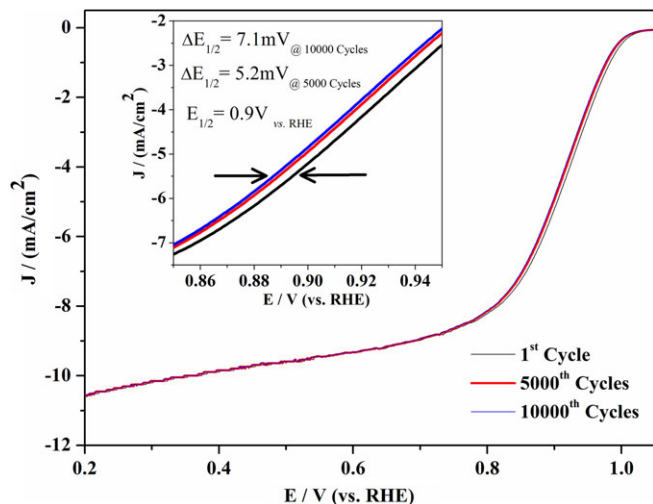


FIGURE 9 ORR polarization plots of the FePc-S-gr electrocatalyst before and after 10,000 potential cycles between 0.2 and 1.1 V (vs. RHE) in an  $O_2$ -saturated KOH solution

130 mV/dec in alkaline solution. This value allows the catalyst to determine the rate-controlling reaction when the four-electron pathway and the two-electron pathway compete. On a metal/metal oxide surface, the rate-determining step is a pseudo- two-electron pathway, which gives a Tafel slope of  $\approx 60$  mV/dec at high potential. However, on a pure metal surface, the first electron transfer is the rate-determining step, resulting in a Tafel slope of  $\approx 120$  mV/dec. Such a high Tafel slope for FePc-S-Gr indicates that the protonation of  $O^{2-}$  is smoother than that of a Pt-based electrocatalyst; however, the protonation of  $O^{2-}$  is the rate-limiting step on the active sites. The small difference in the Tafel slope of FePc-S-Gr indicates that the formed iron oxide at the catalyst surface is insignificant. Therefore, the ORR occurs by the four-electron pathway at the surface of FePc-S-Gr.

Catalyst durability test was carried out by cycling the potentials between 0.2 and 1.1 V (vs. RHE) at 50 mV/s in  $O_2$ -saturated KOH (0.1 mol/L) solution to evaluate the electrochemical stability of the FePc-S-Gr catalysts. More than

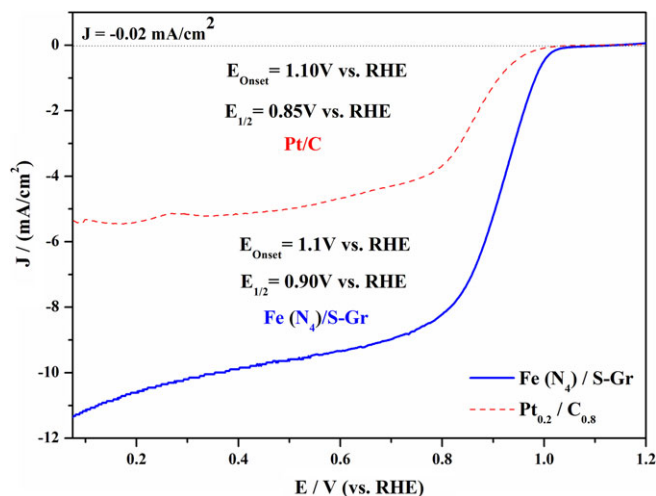


FIGURE 10 Catalyst performance comparison at 1,600 rpm

4,000 cycles are now routinely used in the literature. After 10,000 cycles, the  $E_{1/2}$  of FePc-S-Gr displays a negative shift of only 7.1 mV (Figure 9), which is lower than most reported values.<sup>[42]</sup>

Figure 10 indicates comparison between  $E_{Onset}$  and  $E_{1/2}$  of the FePc-S-Gr electrocatalyst and  $Pt_{0.2}/C_{0.8}$  as a standard reference, from which the higher performance of the new catalyst can be seen.

## 4 | CONCLUSIONS

We demonstrated a new non-precious metal electrocatalyst for the ORR in this paper. The results reflect the intrinsic activity and selectivity of the prepared catalyst. The catalyst exhibited limiting current density and half-wave potential comparable to those of a platinum-based electrocatalyst because of the good mass transport on the catalyst. ORR occurs on the surface of FePc-S-Gr catalyst in an aqueous solution by a multistep reaction. The particle size of the obtained powders is in the nanoscale ( $<10$  nm). The catalytic activity of prepared iron-based catalyst is comparable to that of the Pt/C electrocatalyst used as a reference. The Tafel slope of diffusion-corrected kinetic current density is  $-110$  mV/dec at low current density. The FePc-S-Gr nanostructure exhibits superior durability of performance by using a NPMC in the system.

## ACKNOWLEDGMENT

We thank the staff of the Nanotechnology Research Center, Urmia University, for their assistance with the electrochemical experiments.

## ORCID

Behnam Seyyedi  <https://orcid.org/0000-0001-8084-9108>

## REFERENCES

- [1] C. Soldano, A. Mahmood, E. Dujardin, *Carbon* **2010**, *48*, 2127.
- [2] B. Seyyedi, *Pigm. Resin Technol.* **2017**, *46*, 156.
- [3] W. Yahui, Y. Fuli, Y. Hongwei, Z. Chunbao, C. Yanli, D. Keqiang, *J. Chin. Chem. Soc.* **2013**, *60*, 73.
- [4] B. Seyyedi, *Pigm. Resin Technol.* **2017**, *46*, 267.
- [5] B. Seyyedi, *J. Chin. Chem. Soc.* **2017**, *64*, 1503.
- [6] A. Pullamsetty, R. Sundara, *J. Colloid Interface Sci.* **2016**, *479*, 260.
- [7] M. Pang, C. Li, L. Ding, J. Zhang, D. Su, W. Li, C. Liang, *Ind. Eng. Chem. Res.* **2010**, *49*, 4169.
- [8] Y. Su, Y. Zhu, X. Yang, J. Shen, J. Lu, X. Zhang, J. Chen, C. Li, *Ind. Eng. Chem. Res.* **2013**, *52*, 6076.
- [9] D. Ke-Qiang, *J. Chin. Chem. Soc.* **2010**, *57*, 1309.
- [10] N. Garino, A. Sacco, M. Castellino, J. A. Muñoz-Tabares, A. Chiodoni, V. Agostino, V. Margaria, M. Gerosa, G. Massaglia, M. Quaglio, *ACS Appl. Mater. Interfaces* **2016**, *8*, 4633.
- [11] B. Men, Y. Sun, Y. Tang, L. Zhang, Y. Chen, P. Wan, J. Pan, *Ind. Eng. Chem. Res.* **2015**, *54*, 7415.
- [12] A. Shen, Y. Zou, Q. Wang, R. A. W. Dryfe, X. Huang, S. Dou, L. Dai, S. Wang, *Angew. Chem. Int. Ed.* **2014**, *126*, 10804.
- [13] Z. Liu, X. Lin, J. Y. Lee, W. Zhang, M. Han, L. M. Gan, *Langmuir* **2002**, *18*, 4054.

- [14] G. Liu, H. M. Zhang, M. R. Wang, H. X. Zhong, J. Chen, *J. Power Sources*. **2007**, *172*, 503.
- [15] M. H. Lee, P. S. Wang, J. S. Do, *J. Solid State Electrochem.* **2008**, *12*, 879.
- [16] M. Lefèvre, E. Proietti, F. Jaouen, J. P. Dodelet, *Science* **2009**, *324*, 71.
- [17] S. Ma, G. A. Goenaga, A. V. Call, D. Liu, *Chem. Eur. J.* **2011**, *17*, 2063.
- [18] G. Wu, D. Y. Li, C. S. Dai, D. L. Wang, N. Li, *Langmuir* **2008**, *24*, 3566.
- [19] D. Wang, D. Su, *Energy Environ. Sci.* **2014**, *7*, 576.
- [20] J. Park, Y. Nabaee, T. Hayakawa, M. Kakimoto, *ACS Catal.* **2014**, *4*, 3749.
- [21] N. M. Cantillo, G. A. Goenaga, W. Gao, K. Williams, C. A. Neal, S. Ma, K. L. More, T. A. Zawodzinski, *J. Mater. Chem. A.* **2016**, *4*, 15621.
- [22] H. A. Gasteiger, S. S. Kocha, S. Sompalli, F. T. Wagner, *Appl. Catal. B: Environ.* **2005**, *56*, 9.
- [23] C. Choi, H. Lim, M. Chung, J. Park, H. Shin, H. Kim, S. I. Woo, *J. Am. Chem. Soc.* **2014**, *136*, 9070.
- [24] H. Liang, W. Wei, Z. Wu, X. Feng, K. Müllen, *J. Am. Chem. Soc.* **2013**, *135*, 16002.
- [25] B. Meunier, S. P. D. Visser, S. Shaik, *Chem. Rev.* **2004**, *104*, 3947.
- [26] M. Szybowicz, *J. Mol. Struct.* **2004**, *704*, 107.
- [27] M. Wojdyla, B. Derkowska, W. Bala, *Opt. Appl.* **2005**, *35*, 561.
- [28] W. Bala, M. Wojdyla, M. Rebarz, M. Szybowicz, M. Drozdowski, A. Grodzicki, P. Piszczek, *J. Optoelectron. Mater.* **2009**, *11*, 264.
- [29] T. R. Walton, J. R. Griffith, J. G. O'Rear, *J. Adhes. Sci. Technol.* **1975**, *23*, 665.
- [30] M. Laskoski, M. B. Schear, A. Neal, D. D. Dominguez, H. L. Ricks-Laskoski, J. Hervey, T. M. Keller, *Polymer* **2015**, *67*, 185.
- [31] M. Laskoski, A. Neal, T. M. Keller, D. D. Dominguez, C. A. Klug, A. P. Saab, *J. Polym. Sci. Part A: Polym. Chem.* **2014**, *52*, 1662.
- [32] T. J. Marks, *Science* **1985**, *227*, 881.
- [33] J. Chen, C. Jones, S. Linic, V. Stamenkovic, *ACS Catal.* **2017**, *7*, 6392.
- [34] B. Tunhoo, J. Nukeaw, *Mater. Res. Innov.* **2009**, *13*, 145.
- [35] J. Mack, M. J. Stillman, *Coord. Chem. Rev.* **2001**, *219*, 993.
- [36] A. De Lorenzi, S. Giorgianni, R. Bini, *Molec. Phys.* **1999**, *96*, 101.
- [37] J. Gao, X. Wang, B. Xu, W. Xiuhua, *IET Micro & Nano Letters* **2016**, *11*, 348.
- [38] X. Liu, K. Zhu, J. Tian, O. Tang, Z. Shan, *J. Solid State Electrochem.* **2014**, *18*, 2077.
- [39] D. Li, S. Ge, T. Yuan, J. Gong, B. Huang, W. Tie, W. He, *CrystEngComm.* **2018**, *20*, 2749.
- [40] F. Iwatsu, T. Kobayashi, N. Uyeda, *J. Phys. Chem.* **1980**, *84*, 3223.
- [41] D. Roy, N. M. Das, N. Shakti, P. S. Gupta, *RSC Adv.* **2014**, *4*, 42514.
- [42] A. Holewinski, S. Linic, *J. Electrochem. Soc.* **2012**, *159*, 864.

**How to cite this article:** Seyyedi B, Ahmadi Variani B, Habibi E. Bio-inspired iron/sulfur/graphene nanocomposite and its use in the catalysis of the oxygen reduction reaction at room temperature in alkaline media on a glassy carbon electrode. *J Chin Chem Soc.* 2018;1–7. <https://doi.org/10.1002/jccs.201800326>